ACS APPLIED MATERIALS & INTERFACES

Caltech Library

Subscriber access provided by Caltech Library

Energy, Environmental, and Catalysis Applications

Chalcopyrite ZnSnSb2: A Promising Thermoelectric Material

Ami Nomura, Seongho Choi, Manabu Ishimaru, Atsuko Kosuga, Thomas Chasapis, Saneyuki Ohno, G. Jeffrey Snyder, Yuji Ohishi, Hiroaki Muta, Shinsuke Yamanaka, and Ken Kurosaki

ACS Appl. Mater. Interfaces, **Just Accepted Manuscript** • DOI: 10.1021/acsami.8b16717 • Publication Date (Web): 27 Nov 2018

ACS Publications

is published by the American Chemical Society. 1155 Sixteenth Street N.W., Washington, DC 20036

Chalcopyrite $ZnSnSb_2$: A Promising Thermoelectric Material

Ami Nomura,[†] *Seongho Choi,*[†] *Manabu Ishimaru,*[‡] *Atsuko Kosuga,*[§] *Thomas Chasapis,*[∥] *Saneyuki Ohno,*[∥,⊥] *G. Jeffrey Snyder,*[∥,⊥] *Yuji Ohishi,*[†] *Hiroaki Muta,*[†] *Shinsuke Yamanaka,*[†] *and Ken Kurosaki*[†,#,▽,*]

[†]Graduate School of Engineering, Osaka University, Suita, Osaka 565-0871, Japan

[‡]Department of Materials Science and Engineering, Kyushu Institute of Technology, Tobata, Kitakyushu, Fukuoka 804-8550, Japan

[§]Department of Physical Science, Graduate School of Science, Osaka Prefecture University, Sakai, Osaka 599-8531, Japan

[∥]Department of Materials Science and Engineering, Northwestern University, Evanston, IL 60208, USA

[⊥]Department of Materials science, California Institute of technology, Pasadena, CA, 91125, USA

[#]JST, PRESTO, Kawaguchi, Saitama 332-0012, Japan

[▽]Research Institute of Nuclear Engineering, University of Fukui, Tsuruga, Fukui 914-0055, Japan.

KEYWORDS: thermoelectric, $ZnSnSb_2$, chalcopyrite, band convergence, thermal conductivity, Grüneisen parameter

ABSTRACT: Ternary compounds with a tetragonal chalcopyrite structure such as $CuGaTe_2$ are promising thermoelectric (TE) materials. It has been demonstrated in a various chalcopyrite systems including compounds with quaternary chalcopyrite-like structures that the lattice parameter ratio c/a being exactly 2.00 to have a pseudo-cubic structure is key to increase the degeneracy at the valence band edge and ultimately achieve high thermoelectric performance. Considering the fact that $ZnSnSb_2$ with a chalcopyrite structure is reported to have c/a close to 2.00, it is expected to have multiple valence bands leading to a high *p*-type zT. However, there are no complete investigations on the high temperature TE properties of $ZnSnSb_2$ mainly due to the difficulty of obtaining a single-phase $ZnSnSb_2$. In the present study, pure $ZnSnSb_2$ samples with no impurities are synthesized successfully using a Sn flux-based method and TE properties are characterized up to 585 K. Transport properties and the thermal analysis indicate that the structure of $ZnSnSb_2$ remains chalcopyrite with no order-disorder transition and clearly show that $ZnSnSb_2$ can be made to exhibit a high zT in the low-to-mid temperature range through further optimization.

1. INTRODUCTION

Thermoelectric (TE) conversion is a method of converting heat directly into electricity and is being explored as an effective approach for utilizing exhaust heat. Electric power is generated by exploiting the Seebeck effect for solids, and the performance of the materials being used for TE conversion is evaluated based on a dimensionless figure of merit zT (= $S^2\sigma T/\kappa$,[1] where S is the Seebeck coefficient, σ is the electrical conductivity, κ is the thermal conductivity, and T is the absolute temperature). σ is expressed as $\sigma = en\mu$, where e is the elementary electric charge, n is the carrier concentration, and μ is the carrier mobility. A zT value of 1 is considered as the standard for the commercialization of TE power generation. The parameter $S^2\sigma$ is called the power factor (PF). The thermal conductivity, κ, can be written as $\kappa = \kappa_{lat}+\kappa_{el}$,[1] where κ_{lat} and κ_{el} are the lattice and electronic thermal conductivities, respectively. κ_{el} is related to σ by $\kappa_{el} = LT\sigma$, based on the Wiedemann–Franz law, where L is the Lorenz number. High-performance TE materials should exhibit high PF and low κ_{lat} values.

Chalcopyrite compounds are being explored as novel high-performance TE materials. Cu-based and Ag-based chalcopyrite compounds such as $CuGaTe_2$,[2] $CuInTe_2$,[3] and $AgGaTe_2$[4] are reported to possess a high PF and a low κ_{lat}. The chalcopyrite-like pseudo-cubic compounds $Cu_2CdSnSe_4$[5] and $Cu_2ZnSnSe_4$[6] also exhibit excellent TE performance. In particular, the chalcopyrite compound $CuGaTe_2$, which was discovered by our research group, has an extremely high zT of 1.4 at 950 K.[2] **Figure 1** shows the crystal structure and valence band of chalcopyrite compounds. Chalcopyrite compounds have a tetragonal structure that is composed of two cubic sphalerite-like lattices. When the lattice parameter ratio, c/a, of a chalcopyrite compound is $\fallingdotseq$ 2.00, its valence band is degenerate, with multiple bands at the same energy, as in the case of the pseudo-cubic structure.[7] The value of S increases because of the degeneracy of the valence band

without there being a reduction in the carrier mobility (assuming no intervalley scattering). This results in an increase in *PF*. As a matter of a fact, the *c/a* of $CuGaTe_2$, which shows a high *PF* (1.3 $mW \cdot m^{-1} \cdot K^{-2}$) at 950 K, is almost 2.00, indicating that its valence band should be nearly degenerate.[2,8] This study focuses on $ZnSnSb_2$ as a new chalcopyrite compound. $ZnSnSb_2$ is reported to have a chalcopyrite crystal at low temperatures and transforms to exhibit a sphalerite-like structure at high temperatures, wherein Zn and Sn are placed randomly.[9] It is expected to exhibit a high *PF* because the *c/a* ratio for chalcopyrite $ZnSnSb_2$ should be very close to 2.00.[10] Furthermore, the κ_{lat} value of $ZnSnSb_2$ is expected to be low because, in general, materials that contain heavy elements such as Sn and Sb tend to have low κ_{lat} values.[11].

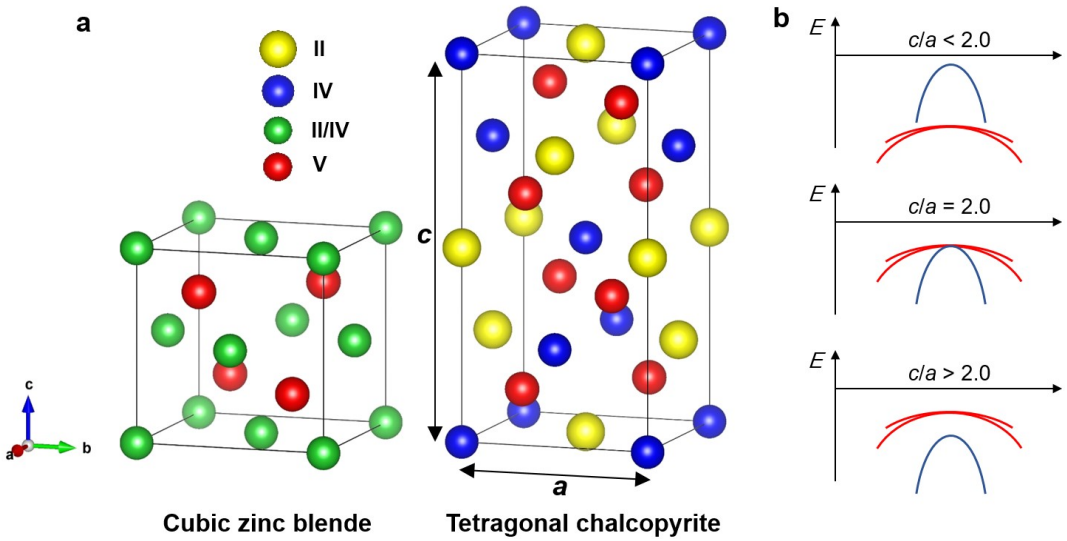

Figure 1. (Color online) (a) Crystal structure of chalcopyrite compounds and (b) dependence of the lattice parameter ratio *c*/*a* on the valence bands position for chalcopyrite compounds. When the *c*/*a* ratio for chalcopyrites is equal to 2.00, the valence bands highly degenerate.

2. EXPERIMENTAL SECTION

It is known that[12] $ZnSnP_2$ is formed by a peritectic reaction and that pure $ZnSnP_2$ can be obtained when Sn is used as the flux and the composition (mol%) of the starting materials corresponds to a Zn/Sn/P ratio of 1:9.2:2. Based on the literature, in this study, the composition of the starting materials (mol%) was taken to be Zn/Sn/Sb = 1:*x*:2 ($x \geqq 9$). First, the starting materials, Zn (99.999%), Sn (99.99%), and Sb (99.999%), were weighed and mixed in the desired ratio. They were then vacuum sealed in a quartz tube, heated till 923 K, and kept at that temperature for 12 h. The tube was then cooled to 533 K and annealed at this temperature for 24 h. The tube was then cooled to room temperature at 0.4 $K \cdot min^{-1}$. This yielded an ingot with an excessive amount of Sn. Next, Sn and $ZnSnSb_2$ were separated based on the low-temperature brittleness of Sn. It is well known that the phase state of Sn is different at room temperature and low temperatures; it is β-Sn at room temperature and extremely brittle α-Sn at low temperatures.[13] Therefore, the ingot was cooled using liquid nitrogen and the brittle Sn and $ZnSnSb_2$ phases were separated manually using a 53 μm mesh sieve. The thus-obtained $ZnSnSb_2$ powder was subjected to spark plasma sintering (SPS-515A, Sumitomo Coal Mining Co.) to produce a bulk sample with a diameter of 10 mm and thickness of 2 mm. The SPS was conducted at 453 K under the pressure of 200 MPa for 15 min in an Ar flow atmosphere. The sintering temperature, 453 K, was determined to suppress the formation of secondary phases during SPS. These undesired reactions might occur in the vicinity of the peritectic reaction, $L + Sn_3Sb_2 = Sn$ at around 500 K, which can be confirmed from the C_P vs T curve (Figure 4). The density, d, of the bulk sample was determined from its weight and dimensions. The relative density of the bulk sample was approximately 85%.

The phases of the powdered and bulk samples were identified using XRD analysis (Ultima-IV, Rigaku Co.). In addition, their crystal structures were characterized using a TEM system (JEM-3000F, JEOL). The elemental distributions within the samples was evaluated quantitatively using EDS (EX-23000BU, JEOL). The Seebeck coefficient, S, and electrical resistivity $\rho\,(=\sigma^{-1})$ were measured using a commercial ZEM-3 system (ULVAC) at temperatures of 300–585 K in a He atmosphere. The Hall coefficient, R_H, was measured by the Van der Pauw method using a custom-built device. The Hall carrier concentration, n_H, and Hall carrier mobility, μ_H, were calculated from the expressions $n_H = 1/|R_H|e$ (e: elementary electric charge) and $\mu_H = |R_H|\sigma$, respectively. The thermal conductivity, κ, was calculated using the expression $\kappa = D_T C_p d$. The thermal diffusivity (D_T), was measured using the flash method (LFA457, NETZSCH); the measurements were performed in an Ar atmosphere. (The result is shown in **Figure S4** in Supporting Information.) The specific heat under constant pressure, C_p, was measured using differential scanning calorimetry (STA449C, NETZSCH). The sound velocity of the samples was measured by the ultrasonic pulse echo method; the measurements were performed in air at room temperature using 10 MHz ultrasonic waves.

In order to investigate the optical band gap, diffuse reflectance infrared Fourier transform spectroscopy measurements were performed using a Nicolet 6700 FTIR system fitted with a Praying Mantis™ diffuse reflectance attachment (Harrick). The optical absorption coefficient, α, was determined using the Kubelka-Munk function $F(R) = (1\text{-}R)^2/(2R) = \alpha/K$, where R is the measured diffuse reflectance and K is the scattering coefficient.

The electron state of $ZnSnSb_2$ was calculated using the Vienna ab-initio simulation package (VASP). The projector augmented wave method (PAW) was used for the calculations, which were based on the density functional theory (DFT). The Perdew-Burke-Ernzerhof generalized

gradient approximation (GGA-PBE) and the modified Becke-Johnson exchange potential in combination with the local density approximation correlation (mBJ-LDA) were used for the simulations of the structural relaxation and band structure, respectively. The cutoff energy was 500 eV, and the mesh number at point k was $9 \times 9 \times 9$.

3. RESULTS AND DISCUSSION

While $CuGaTe_2$ can be synthesized simply by melting at the stoichiometric ratio of Cu/Ga/Te = 1:1:2, the synthesis of pure $ZnSnSb_2$ is extremely difficult to achieve as it involves a peritectic reaction.[2,9,14,15] Hence, the TE properties of $ZnSnSb_2$ have not been well studied previously. Therefore, in this study, we synthesize pure $ZnSnSb_2$ using a Sn flux-based method that has been used for synthesizing single-phase $ZnSnP_2$[12] and evaluate its TE properties up to 585 K.

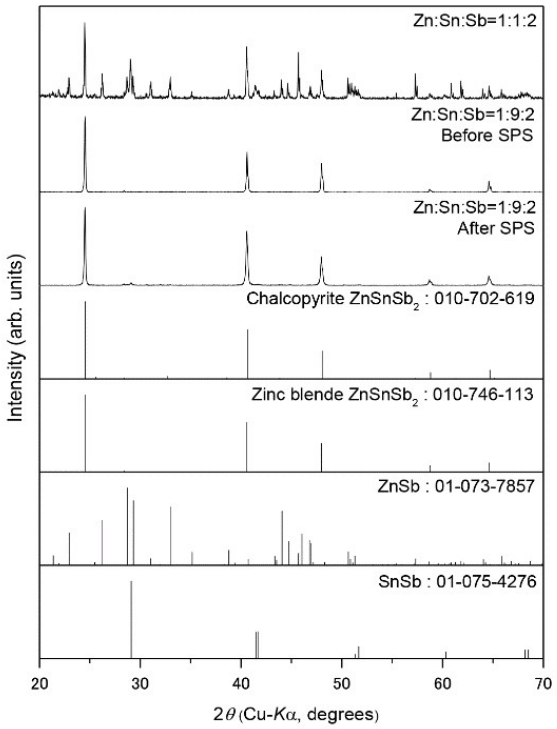

Figure 2. XRD patterns for the samples, together with the literature data of chalcopyrite $ZnSnSb_2$, zinc blende $ZnSnSb_2$, ZnSb, and SnSb. Pure $ZnSnSb_2$ was obtained by a Sn flux method when the composition of the starting materials (mol %) was Zn:Sn:Sb＝1:9:2.

Table 1. Lattice parameters a and c, lattice parameter ratio c/a, theoretical density d_{th}, and measured density d_m for $ZnSnSb_2$. All parameters were obtained at room temperature.

	a (Å)	c (Å)	c/a	d_{th} (g/cm^3)	d_m (g/cm^3)	%TD
This work	6.284(2)	12.556(8)	1.998	5.747	4.880	85
Ref.[10]	6.275	12.550	2.000	5.747	-	-

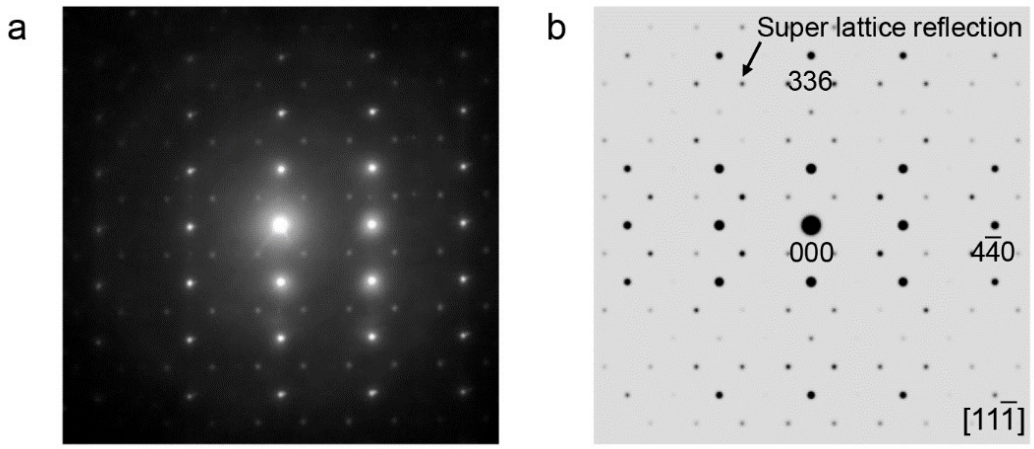

Figure 3. (Color online) (a) Electron diffraction pattern and (b) simulated EDP of $ZnSnSb_2$ along <11$\bar{1}$> direction. The crystal structure of $ZnSnSb_2$ can be identified as a chalcopyrite type because superlattice reflections associated with the chalcopyrite structure can be confirmed in addition to the basic lattice reflection of the sphalerite structure.

Figure 2 shows the X-ray diffraction (XRD) patterns for the powdered and bulk samples. As can be seen, a starting composition (mol%) of Zn/Sn/Sb = 1:1:2 results in the formation of large amounts of ZnSb and SnSb as impurities, in addition to $ZnSnSb_2$. However, single-phase $ZnSnSb_2$ free of impurities is synthesized successfully by adjusting the ratio of the starting materials (mol%) to Zn/Sn/Sb = 1:9:2 and removing the excessive Sn. The lattice parameter ratio of $ZnSnSb_2$, c/a, is 1.998 and nearly equals to that reported in the literature (See Table 1).[10] The results of the quantitative elemental analysis performed using energy-dispersive X-ray spectroscopy (EDS) show that the composition of $ZnSnSb_2$ is essentially Zn/Sn/Sb = 1:1:2 (these results are shown in **Figure S1** in Supporting Information). It is not easy to determine whether

$ZnSnSb_2$ is chalcopyrite-like or sphalerite-like only by XRD patterns because the low-intensity peaks characterizing chalcopyrite structure overlap peaks from the impurities ZnSb and SnSb.[9] Therefore, the samples are evaluated using transmission electron microscopy (TEM). **Figure 3a** shows the electron diffraction pattern (EDP) of the powdered sample obtained along the <111> direction using TEM. In the EDP, several superlattice reflections can be observed, in addition to the fundamental lattice reflection of the sphalerite structure. This confirms that the crystal structure of the synthesized sample is chalcopyrite. Further, the simulated EDP for the chalcopyrite structure (see **Figure 3b**) is in good agreement with the experimental results.

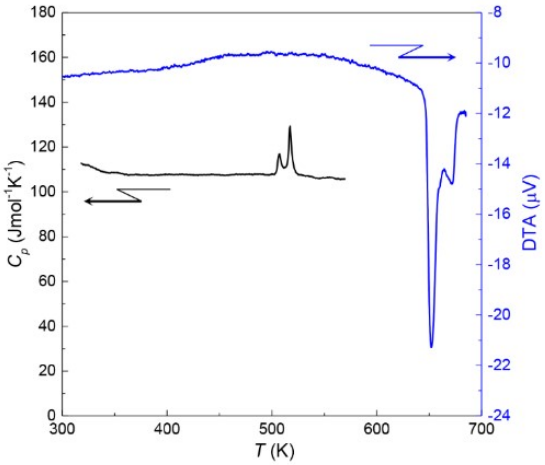

Figure 4. (Color online) Temperature dependence of heat capacity C_p and the result of DTA of $ZnSnSb_2$. The two peaks in the C_P curve are attributed to chemical reactions of impurities. Chalcopyrite $ZnSnSb_2$ is stable and there is no order-disorder (from chalcopyrite to sphalerite) phase transition before it decomposes.

In contrast to the reported order-disorder transition in ref (9), we experimentally observe no order-disorder transition and confirm that the chalcopyrite structure remains up to its decomposition temperature as it's theoretically shown in ref (16). **Figure 4** shows the temperature dependence of heat capacity (C_p) measured by a differential scanning calorimeter (DSC) and the result of differential thermal analysis (DTA). Two peaks are present for C_p in the

500–530 K range. According to the Sn-Sb binary phase diagram,[17] the peritectic reaction, L + Sn_3Sb_2 = Sn occurs at 516 K, and the melting point for Sn is close to this temperature. Rincon[16] calculated the order-disorder phase transition temperature (T_c) in ternary chalcopyrite compounds from the view point of the band gap difference between the order and disorder phases. The calculated T_c of the other pnictides analogues such as $ZnSnP_2$ and $ZnSnAs_2$ were consistent with the experimentally observed values.[18] As for $ZnSnSb_2$, the calculated T_c was 759 K, which is higher than the decomposition temperature confirmed in this work. Therefore, we conclude that the peaks around 500–530 K in the C_P curve are attributed to Sn melting and the peritectic reaction, L + Sn_3Sb_2 = Sn since DSC is more sensitive than DTA. The peak observed along the DTA curve starting at around 600 K is related to the decomposition of $ZnSnSb_2$ to ZnSb and SnSb.

Generally, the porosity of a material has a significant effect on its σ and κ values as well as the velocity of sound in the material, and corrections based on the porosity are necessary for ensuring the accuracy of the obtained values of the physical parameters. In this study, we use the Maxwell-Eucken equations to correct for the porosity in the case of the electrical resistivity and thermal conductivity. The Maxwell-Eucken equations are as follows:[19,20]

$$\sigma_0 = \sigma_P \frac{(1 + \beta P)}{(1 - P)} \quad (1)$$

$$\kappa_0 = \kappa_P \frac{(1 + \beta P)}{(1 - P)} \quad (2)$$

where σ_0 and κ_0 are the corrected electrical and thermal conductivities assuming no porosity, σ_P and κ_P are the electrical and thermal conductivity at porosity P with the parameter of β depending on the shape of the pores assumed to be 1.4 for this study.[21] The relative density of the

bulk samples for transport measurements is approximately 85%. This low relative density is due to the low sintering temperature during SPS, which is determined to avoid the formation of secondary phases. Although we applied the highest pressure of 200 MPa as far as we can during SPS, it was not enough to get high density. On the other hand, because the sound velocity and porosity exhibit an inverse relationship,[22] multiple bulk samples with varying porosities are prepared, and the sound velocities of these samples are measured and extrapolated linearly to determine the sound velocity at zero porosity. The porosity dependence of S is not considered as no porosity dependence in Seebeck is expected.

The high temperature electronic and thermal transport properties of $ZnSnSb_2$ are measured for the first time in this study. **Figure 5a** and **5b** show the temperature dependences of S and ρ, respectively, for $ZnSnSb_2$. It can be seen that ρ increases slightly with an increase in the temperature; this is in keeping with previously reported results.[9,23] In this study, the ρ values as measured at room temperature are slightly greater than those reported previously possibly due to the effect of impurities.[24] Further, the ρ values are very small, at less than 1.0 mΩ·cm, for every temperature range investigated. S increases with the temperature, in keeping with the literature data of low temperature.[9] Positive S indicates that $ZnSnSb_2$ exhibits p-type conduction and it's confirmed by the Hall effect measurements show that the positive Hall coefficient. **Figure 5c** and **5d** show the temperature dependences of the Hall carrier mobility, μ_H, and Hall carrier concentration, n_H, respectively. The primary carrier scattering mode in $ZnSnSb_2$ is assumed to be acoustic phonon scattering as many other thermoelectrics because μ_H decreases proportional to $T^{-1.5}$.[25] The n_H remains constant regardless of the temperature and its value is approximately 2.2×10^{20} cm^{-3}.

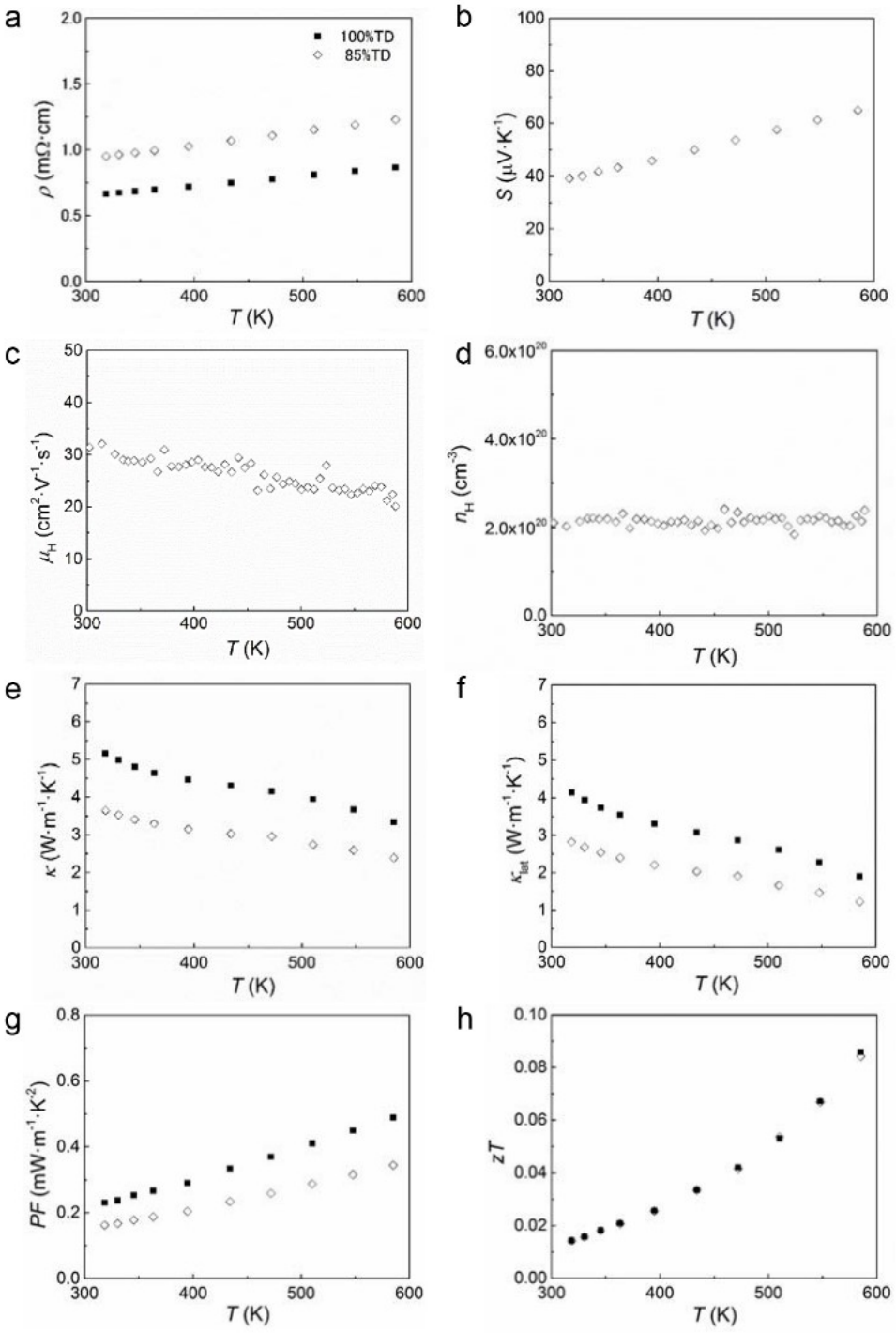

Figure 5. Temperature dependences of thermoelectric transport properties of $ZnSnSb_2$. (a) electrical resistivity ρ, (b) Seebeck coefficient S, (c) Hall carrier mobility μ_H, (d) Hall carrier concentration n_H, (e) thermal conductivity κ, (f) lattice thermal conductivity κ_{lat}, (g) power factor PF, and (h) dimensionless figure of merit zT.

Figure 5e and **5f** show the temperature dependences of κ and κ_{lat}, respectively. The κ value of $ZnSnSb_2$ for 100 %T.D. is 5.2 $W \cdot m^{-1} \cdot K^{-1}$ at room temperature and 3.3 $W \cdot m^{-1} \cdot K^{-1}$ at 585 K. κ_{lat} is estimated as the difference between κ and κ_{el} ($\kappa_{lat} = \kappa - \kappa_{el}$) where κ_{el} is calculated based on the Wiedemann–Franz law. The value of the Lorenz number, L, used here is calculated from the physical parameters determined in this study. The contribution of κ_{el} to κ is approximately 20% at room temperature and increases with an increase in the temperature, reaching up to 43% at 585 K. The κ_{lat} value of $ZnSnSb_2$ for 100 %T.D. is 4.1 $W \cdot m^{-1} \cdot K^{-1}$ at room temperature and decreases in proportion to T^{-1} down to 1.9 $W \cdot m^{-1} \cdot K^{-1}$ at 585 K due to the Umklapp scattering. Slack showed that κ_{lat} can be expressed as follows:[11,26]

$$\kappa_{lat} = A \frac{M \delta \theta^3}{N^{2/3} \gamma^2} \frac{1}{T} \tag{3}$$

The Debye temperature, θ, and the average sound velocity, v_m, are given by the following equations:

$$\theta = v_m \left(\frac{h}{k_B} \right) \left(\frac{3 n N_A d}{4 \pi M_W} \right)^{\frac{1}{3}} \tag{4}$$

$$v_m^{-3} = \frac{\left(v_l^{-3} + 2 v_t^{-3} \right)}{3} \tag{5}$$

where A, M, δ^3, N, γ, k_B, N_A, h, n, M_w, v_l, and v_t are a constant independent of the material in question, the average atomic mass, average atomic volume, the number of atoms per unit cell, Grüneisen parameter, Boltzmann constant, Avogadro constant, Planck constant, the number of atoms per molecule, molecular mass, longitudinal speed of sound, and transverse speed of sound, respectively. **Table 2** shows the v_m and θ values for $ZnSnSb_2$ and $CuGaTe_2$. The porosity correction is also applied to the data of speed of sounds. Generally, increasing anharmonicity of

the lattice vibrations (increasing Grüneisen parameter, γ) leads to the reduction of κ_{lat}.[27] Equation (3) shows that κ_{lat} is proportional to $M\delta\theta^3/\gamma^2$ for the same crystal structure at a constant temperature. **Figure 6** shows $M\delta\theta^3$ dependency on κ_{lat} for a various chalcopyrite compounds at room temperature.[2,3,7,28–30] The κ_{lat} increases with $M\delta\theta^3$ in an essentially linear manner for most of chalcopyrite compounds except $ZnSnSb_2$. $ZnSnSb_2$ has a relatively lower κ_{lat} compared to the other chalcopyrite compounds mainly because of slightly larger γ than those of other chalcopyrite compounds.

Table 2. Longitudinal sound velocity v_l, transverse sound velocity v_t, average sound velocity v_m, coefficient of volumetric thermal expansion α_v, bulk modulus B, Grüneisen parameter γ, and Debye temperature θ of $ZnSnSb_2$ and $CuGaTe_2$.[2]

Parameter	$ZnSnSb_2$	$CuGaTe_2$[2]
v_l ($m \cdot s^{-1}$)	4028	3817
v_t ($m \cdot s^{-1}$)	2302	2072
v_m ($m \cdot s^{-1}$)	2558	2312
θ (K)	243	229
B (GPa)	52.6	51.5
α_v (K^{-1})	3.1×10^{-5}	3.0×10^{-5}
γ	1.2	1.0

To experimentally confirm the γ value for $ZnSnSb_2$, high-temperature XRD measurements (the results are shown in **Figure S2** and **S3** in Supporting Information) are conducted. With the volumetric thermal expansion, α_v, calculated from the temperature dependency of the lattice parameters and following equations:[31,32]

$$\gamma = \frac{\alpha_v B v_m}{C_V} \quad (6)$$

$$B = d\left(v_l^{\,2} - \frac{4}{3} v_t^{\,2} \right) \tag{7}$$

where B is the bulk modulus, C_v is the specific heat for a constant volume obtained based on the Dulong–Petit law ($C_v = 3nR$ where R is the gas constant), γ value for $ZnSnSb_2$ is determined and listed in Table 2 with the values of $CuGaTe_2$. The value of γ is 1.2 for $ZnSnSb_2$ and is larger than that for $CuGaTe_2$ (γ = 1.0[2]), suggesting that the anharmonicity of the lattice vibrations in $ZnSnSb_2$ is greater compared to the other chalcopyrite compounds and resulting in its lower κ_{lat} value. The glassy limit κ_{lat} value, κ_{glass}, corresponds to the assumption that all the phonons have the smallest mean free path, is given by the following equation:[33-34]

$$\kappa_{glass} \approx 1.2 \frac{k_B v_m}{\delta^2} \tag{8}$$

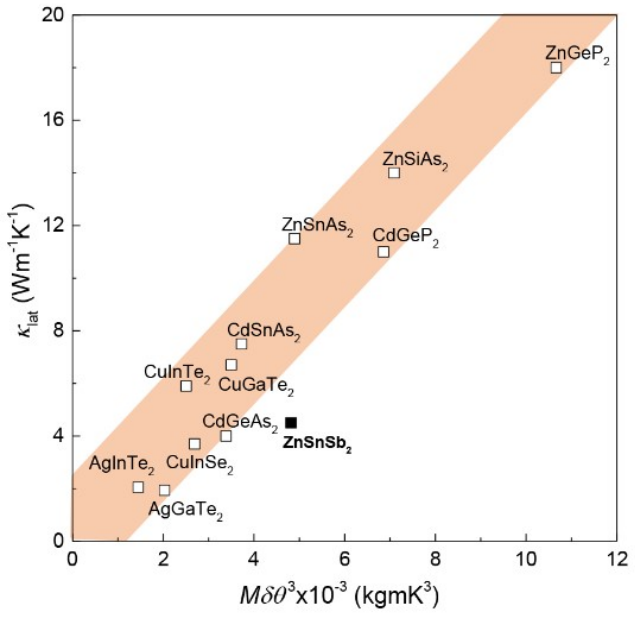

Figure 6. (Color online) Lattice thermal conductivity κ_{lat} of chalcopyrite compounds as a function of the scaling parameter $M\delta\theta^3$, where M is average mass per atom, δ^3 is average volume per atom, and θ is Debye temperature.[2,3,7,29,30,32] κ_{lat} increases as $M\delta\theta^3$ increases in an essentially linear manner for chalcopyrite compounds except for $ZnSnSb_2$ having large Grüneisen parameter γ and low κ_{lat} compared to other chalcopyrite compounds.

This equation is established based on the model proposed by Cahill et al[33], and can be applied to evaluate the glassy limit of κ_{lat} of various crystals and glasses such as solid solutions of GeTe and $AgSbSe_2$ [35]. Equation (8) yields $\kappa_{glass} = 0.43\ W \cdot m^{-1} \cdot K^{-1}$ for $ZnSnSb_2$. Since the measured value of κ_{lat} is 1.7 $W \cdot m^{-1} \cdot K^{-1}$ at 585 K, this result indicates that κ_{lat} can be reduced further.

Figure 5g and **5h** show the temperature dependences of *PF* and *zT*, respectively, for $ZnSnSb_2$. *PF* and *zT* monotonically increase as a function of temperature and achieve 0.49 $mW \cdot m^{-1} \cdot K^{-2}$ (ρ = 0.86 $m\Omega \cdot cm$ and S = 64.9 $\mu V \cdot K^{-1}$) and 0.086, respectively, at 585 K.

To examine the best possible *zT* from $ZnSnSb_2$, here we analyze the carrier concentration dependence of *zT* using the single parabolic band (SPB) model as it's shown in $CuGaTe_2$.[36] In the SPB model, assuming account phonon scattering, n_H, S, μ_H, and L are given by the following equations:[36-37]

$$n_H = 4\pi\left(\frac{2m^* k_B T}{h^2}\right)^{3/2} \frac{F_{1/2}(\eta)}{r_H} \tag{9}$$

$$S(\eta) = \frac{k_B}{e}\left[\frac{(2+\lambda)F_{(\lambda+1)}(\eta)}{(1+\lambda)F_\lambda(\eta)} - \eta\right] \tag{10}$$

$$\mu_H = \frac{e\pi\hbar^4}{\sqrt{2}(k_B T)^{3/2}} \frac{C_{11}}{E_{def}^2 (m^*)^{5/2}} \frac{(1/2+2\lambda)F_{2\lambda-1/2}(\eta)}{(1+\lambda)F_\lambda(\eta)} \tag{11}$$

$$L = \left(\frac{k_B}{e}\right)^2 \frac{(1+\lambda)(3+\lambda)F_\lambda(\eta)F_{\lambda+2}(\eta) - (2+\lambda)^2 F_{\lambda+1}(\eta)^2}{(1+\lambda)^2 F_\lambda(\eta)^2} \tag{12}$$

$$F_j(\eta) = \int_0^\infty \frac{\xi^j d\xi}{1 + Exp[\xi - \eta]} \tag{13}$$

where $F_j(\eta)$ is the Fermi integral; η is the reduced Fermi level; e is the elementary electric charge; m^* is the effective mass of the state density; E_{def} is the deformation potential coefficient, which is indicative of the intensity of acoustic phonon scattering; C_{11} is the elastic constant for

longitudinal vibrations ($C_{11} = v_l^2 d$);[38] and r_H is the Hall factor, which is taken to be unity in this study. λ represents the energy dependence of the carrier relaxation time and assumed to be 0 taking acoustic phonon scattering alone into account. The values employed in this study for SPB analysis and the determined parameters for $ZnSnSb_2$ are listed in Table 3. The m^* value for $ZnSnSb_2$ ($m^* = 0.66m_e$) is nearly equal to that for $CuGaTe_2$ ($m^* = 0.65m_e$[36]).

Table 3. Hall carrier concentration n_H, Seebeck coefficient S, Hall carrier mobility μ_H, elastic constant for longitudinal vibrations C_{11}, effective mass of density of state m^*, Lorenz number L, and deformation potential coefficient E_{def} for $ZnSnSb_2$.

Parameter	Temperature (K)	
	319	585
n_H ($c \cdot m^{-3}$)	2.2×10^{20}	2.2×10^{20}
S ($\mu V \cdot K^{-1}$)	39.2	64.9
μ_H ($cm^2 \cdot V^{-1} \cdot s^{-1}$)	29.8	21.6
C_{11} (GPa)	93	93
m^*	0.66 m_e	0.60 m_e
L ($W \cdot \Omega \cdot K^{-2}$)	2.30×10^{-8}	2.12×10^{-8}
E_{def} (eV)	15.5	14.9

Predicted zT with κ_{glass} based on SPB analysis indicates the promising TE properties of $ZnSnSb_2$ motivation further optimization of this material. **Figure 7** shows the carrier concentration dependence of zT as determined using the SPB model for $ZnSnSb_2$. As is the case for κ_{lat}, the empirical values obtained in this study are used for the analysis and κ_{el} is calculated using the Wiedemann–Franz law. The zT of the sample also increases with the temperature, with zT predicted to be 0.24 when $n_H = 2\times10^{19}$ cm^{-3} at 585 K. In addition, the maximum zT is 0.7 when $\kappa_{glass} = 0.43$ $W \cdot m^{-1} \cdot K^{-1}$ (as determined by Equation (8)).

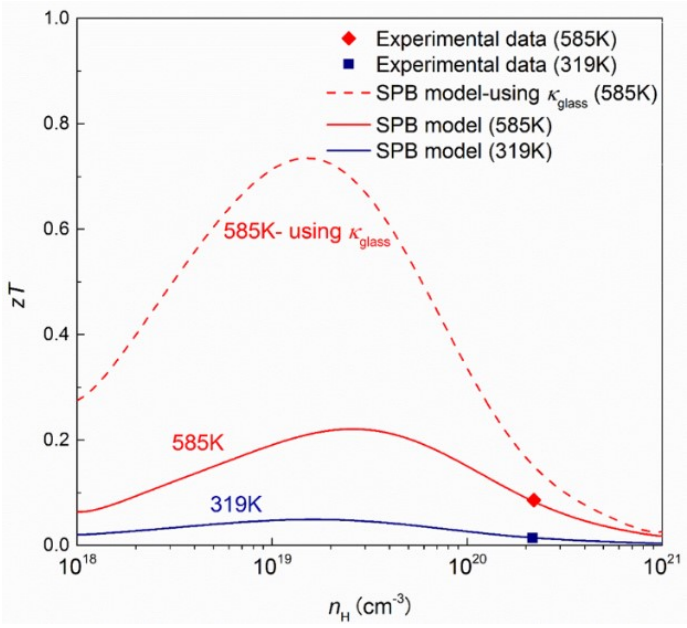

Figure 7. (Color online) Hall carrier concentration n_H dependence of dimensionless figure of merit zT of $ZnSnSb_2$ determined by the single parabolic band model. Here, we used measured κ_{lat} and estimated κ_{glass} for calculating zT. When the optimal carrier concentration and κ_{glass} are achieved for $ZnSnSb_2$, the maximum zT reaches 0.73 at 585 K.

As it's observed in other chalcopyrite-like compounds, the key to obtain large thermopower is the ratio of c/a being almost exactly 2.00. **Figure 8a** and **8b** show the band structure and density of state (DOS), respectively, for the chalcopyrite $ZnSnSb_2$ as determined through ab-initio calculations. The figures show that the valence bands degenerate. It has been reported that the PF and zT increase with increasing Fermi pocket degeneracy for various TE materials, including PbTe,[39] $CoSb_3$,[40] and Mg_2Si-Mg_2Sn.[41] This is owing to the fact that the value of S (for a given n) increases with the degeneracy of the light bands, with the carrier mobility not being affected.[42] Figure 8b shows that the valence band of the DOS near the Fermi level exhibits a steep slope. According to Mott's theory, the steeper is the DOS slope near the Fermi level, the greater is S.[43] As shown in Figure 8a, a direct transition band gap is predicted by DFT between Γ–Γ ($E_{g,\Gamma-\Gamma}$ =

0.28 eV) and an indirect transition band gap predicted between Γ–X ($E_{g,\Gamma-X}$ = 0.59 eV).

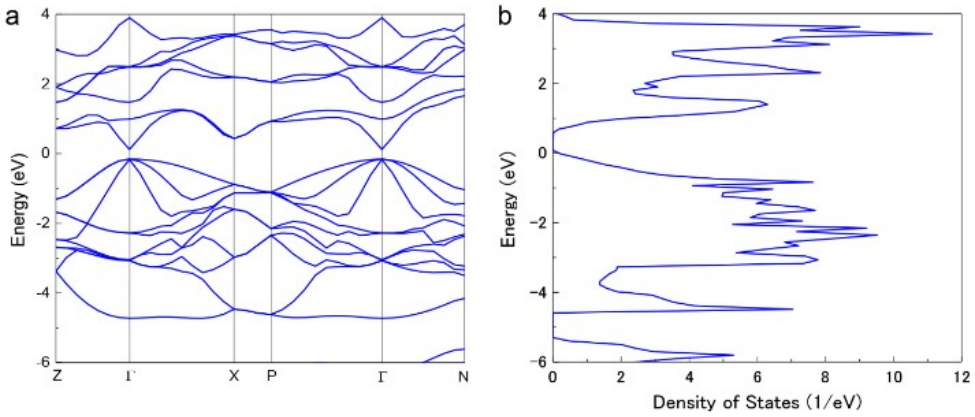

Figure 8. (Color online) DFT-calculated electronic state of $ZnSnSb_2$. (a) Band structure and (b) density of state. The band structure of $ZnSnSb_2$ represents that the valence bands highly degenerate at point Γ.

While the valence band of chalcopyrite structure is degenerate at the band edge when c/a = 2.00, the Materials Project[44] shows that a large offset at Γ point when c/a is only slightly off from the exact 2.00. Therefore, to experimentally evaluate the band gaps and confirm the band convergence, the optical absorption coefficient of the powder-form $ZnSnSb_2$ sample is determined through Fourier transform infrared spectroscopy (FTIR) measurements. **Figure 9** shows the optical absorption coefficient, α, of the sample at room temperature. Two transitions, one at 0.16 eV and another at 0.33 eV, can be seen in the figure. This could be due to the three valence bands of $ZnSnSb_2$ not being degenerate at the Γ point, and the two transitions observed in Figure 9 correspond to the two Γ-Γ transitions, as observed in Ge.[45] In this case, $ZnSnSb_2$ can be even better by tuning the c/a via solid solution for example.

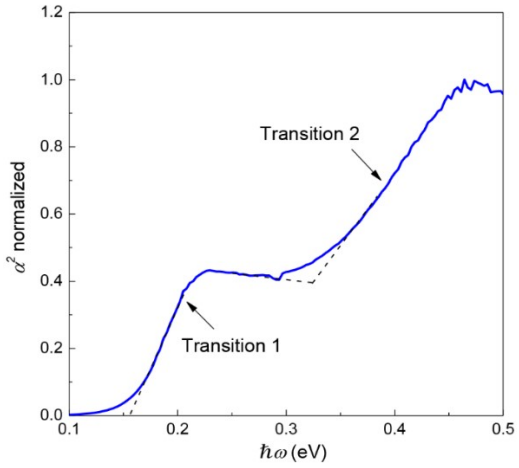

Figure 9. (Color online) Optical absorption coefficient α as a function of photon energy for $ZnSnSb_2$ obtained at room temperature, which suggests two distinct transitions.

4. CONCLUSIONS

The pure chalcopyrite $ZnSnSb_2$ with c/a nearly equal to 2.00 is successfully synthesized using the Sn flux method. Further, our ab-initio calculations show that the valence band of $ZnSnSb_2$ degenerates at point Γ and that the DOS near the Fermi level has a steep slope. Optical band gap measurements indicate that $ZnSnSb_2$ has two band gaps, 0.16 eV and 0.33 eV, and they would correspond to an intra- and inter-band transitions at point Γ, occurred when c/a is only slightly off from the exact 2.00 (c/a = 1.998). The Grüneisen parameter, γ, of $ZnSnSb_2$ is 1.2, which is higher than those for other chalcopyrite compounds; this results in a low κ_{lat}. Analysis based on the SPB model reveals that the zT for $ZnSnSb_2$ is 0.24 at 585 K and $n_H = 2\times10^{19}$ cm^{-3} (zT = 0.7 if $\kappa = \kappa_{glass}$). The zT value can be increased by (1) adjusting the lattice parameter ratio (c/a) to tune the band convergence, (2) optimizing the carrier concentration, and (3) substituting other elements to reduce κ_{lat} further.

ASSOCIATED CONTENT

Supporting Information

The Supporting Information is available free of charge on the ACS Publications website.

FE-SEM and EDX images of the $ZnSnSb_2$ samples, high-temperature XRD patterns for powdered $ZnSnSb_2$, temperature dependence of the lattice parameters obtained by high-temperature XRD analysis, and temperature dependence of thermal diffusivity.

AUTHOR INFORMATION

Corresponding Authors

*E-mail: kurosaki@see.eng.osaka-u.ac.jp (K.K.).

ORCID

Ken Kurosaki: 0000-0002-3015-3206

Seongho Choi: 0000-0001-8891-5202

Saneyuki Ohno: 0000-0001-8192-996X

Jeff Snyder: 0000-0003-1414-8682

Notes

The authors declare no competing financial interest.

Author Contributions

The manuscript was written through contributions of all authors. All authors have given approval to the final version of the manuscript.

ACKNOWLEDGMENTS

Part of this study was funded by JST, PRESTO Grant Number JPMJPR15R1.

REFERENCES

(1) Snyder, G. J.; Toberer, E. S. Complex Thermoelectric Materials. *Nat. Mater.* **2008,** *7* (2), 105-114.

(2) Plirdpring, T.; Kurosaki, K.; Kosuga, A.; Day, T.; Firdosy, S.; Ravi, V.; Snyder, G. J.; Harnwunggmoung, A.; Sugahara, T.; Ohishi, Y.; Muta, H.; Yamanaka, S. Chalcopyrite $CuGaTe_2$: A High-Efficiency Bulk Thermoelectric Material. *Adv. Mater.* **2012,** *24* (27), 3622-3626.

(3) Liu, R.; Xi, L.; Liu, H.; Shi, X.; Zhang, W.; Chen, L. Ternary Compound $CuInTe_2$: A Promising Thermoelectric Material with Diamond-like Structure. *Chem. Comm.* **2012,** *48* (32), 3818-3820.

(4) Yusufu, A.; Kurosaki, K.; Kosuga, A.; Sugahara, T.; Ohishi, Y.; Muta, H.; Yamanaka, S. Thermoelectric Properties of $Ag_{1-x}GaTe_2$ with Chalcopyrite Structure. *Appl. Phys. Lett.* **2011,** *99* (6), 061902.

(5) Liu, M.-L.; Chen, I. W.; Huang, F.-Q.; Chen, L.-D. Improved Thermoelectric Properties of Cu-Doped Quaternary Chalcogenides of $Cu_2CdSnSe_4$. *Adv. Mater.* **2009,** *21* (37), 3808-3812.

(6) Liu, M.-L.; Huang, F.-Q.; Chen, L.-D.; Chen, I.-W. A Wide-band-gap *p*-Type Thermoelectric Material based on Quaternary Chalcogenides of Cu_2ZnSnQ_4 (Q=S, Se). *Appl. Phys. Lett.* **2009,** *94* (20), 202103.

(7) Zhang, J.; Liu, R.; Cheng, N.; Zhang, Y.; Yang, J.; Uher, C.; Shi, X.; Chen, L.; Zhang, W. High-Performance Pseudocubic Thermoelectric Materials from Non-Cubic Chalcopyrite Compounds. *Adv. Mater.* **2014,** *26* (23), 3848-3853.

(8) Yang, J.; Yan, Y.; Wang, Y. X.; Yang, G. Improved Thermoelectric Performance of $CuGaTe_2$ with Convergence of Band Valleys: A first-principles Study. *RSC Advances* **2014,** *4* (54), 28714-28720.

(9) Tengå, A.; García-García, F. J.; Mikhaylushkin, A. S.; Espinosa-Arronte, B.; Andersson, M.; Häussermann, U. Sphalerite−Chalcopyrite Polymorphism in Semimetallic $ZnSnSb_2$. *Chem. Mater.* **2005,** *17* (24), 6080-6085.

(10) Vaipolin, A. A., Kradinova, L.V., Prochukhan, V.D. X-ray Defraction Study of the Semiconducting Alloy $ZnSnSb_2$. *Kristallografiya* **1970,** *15*, 820.

(11) Slack, G. A. The Thermal Conductivity of Nonmetallic Crystals. In *Solid State Physics*; Ehrenreich, H.; Seitz, F.; Turnbull, D., Eds.; Academic Press: **1979**; pp 1-71.

(12) Nakatsuka, S.; Nakamoto, H.; Nose, Y.; Uda, T.; Shirai, Y. Bulk Crystal Growth and Characterization of $ZnSnP_2$ Compound Semiconductor by Flux Method. *physica status solidi c* **2015,** *12* (6), 520-523.

(13) Eckert, A. Organ Pipes and Tin Pest. *Mater. Corros.* **2008,** *59* (3), 254-260.

(14) Scott, W. Preparation and Some Properties of ZnSnSb2. *J. Appl. Phys.* **1973,** *44* (11), 5165-5166.

(15) Kuhn, B.; Kaefer, W.; Fess, K.; Friemelt, K.; Turner, C.; Wendl, M.; Bucher, E. Thermoelectric Properties of $CuIn_{1-x}Ga_xTe_2$ Single Crystals. *physica status solidi (a)* **1997,** *162* (2), 661-671.

(16) Rinco´n, C. Order-disorder Transition in Ternary Chalcopyrite Compounds and Pseudobinary Alloys. *Phys. Rev. B* **1992,** *45* (22), 12716-12719.

(17) Chen, S.-W.; Chen, C.-C.; Gierlotka, W.; Zi, A.-R.; Chen, P.-Y.; Wu, H.-J. Phase Equilibria of the Sn-Sb Binary System. *J. Electro. Mater.* **2008,** *37* (7), 992-1002.

(18) Rincón, C. On the Order-disorder Phase Transition in Ternary Compounds. *Solid State Commun.* **1987,** *64* (5), 663-665.

(19) Smith, D. S.; Alzina, A.; Bourret, J.; Nait-Ali, B.; Pennec, F.; Tessier-Doyen, N.; Otsu, K.; Matsubara, H.; Elser, P.; Gonzenbach, U. T. Thermal Conductivity of Porous Materials. *J. Mater. Res.* **2013,** *28* (17), 2260-2272.

(20) Eucken, A. Allgemeine Gesetzmäßigkeiten für das Wärmeleitvermögen verschiedener Stoffarten und Aggregatzustände. *Forschung auf dem Gebiet des Ingenieurwesens A* **1940,** *11* (1), 6-20.

(21) Biancheria, A. The Effect of Porosity on Thermal Conductivity of Ceramic Bodies. *Trans. Am. Nucl. Soc.* **1966,** *9* (1), 15.

(22) Soga, N.; Schreiber, E. Porosity Dependence of Sound Velocity and Poisson's Ratio for Polycrystalline MgO Determined by Resonant Sphere Method. *J. Am. Ceram. Soc.* **1968,** *51* (8), 465-467.

(23) Kradinova, L. V.; Voronina, T. I. On Electro-Physical Properties of $ZnSnSb_2$. *physica status solidi (b)* **1969,** *32* (2), K173-K174.

(24) Ohno, S.; Aydemir, U.; Amsler, M.; Pöhls, J.-H.; Chanakian, S.; Zevalkink, A.; White, M. A.; Bux, S. K.; Wolverton, C.; Snyder, G. J. Achieving $zT > 1$ in Inexpensive Zintl Phase $Ca_9Zn_{4+x}Sb_9$ by Phase Boundary Mapping. *Adv. Funct. Mater.* **2017,** *27* (20), 1606361.

(25) Pei, Y.; Gibbs, Z. M.; Gloskovskii, A.; Balke, B.; Zeier, W. G.; Snyder, G. J. Optimum Carrier Concentration in *n*-Type PbTe Thermoelectrics. *Adv. Energy Mater.* **2014,** *4* (13), 1400486.

(26) Anderson, O. L. A Simplified Method for Calculating the Debye Temperature from Elastic Constants. *J. Phys. Chem. Solids* **1963,** *24* (7), 909-917.

(27) Zeier, W. G.; Zevalkink, A.; Gibbs, Z. M.; Hautier, G.; Kanatzidis, M. G.; Snyder, G. J. Thinking Like a Chemist: Intuition in Thermoelectric Materials. *Angew. Chem. Int. Ed.* **2016,** *55* (24), 6826-6841.

(28) Bohmhammel, K.; Deus, P.; Kühn, G.; Möllee, W. Specific Heat, Debye Temperature, and belated Properties of Chalcopyrite Semiconducting Compounds $CuGaSe_2$, $CuGaTe_2$, and $CuInTe_2$. *physica status solidi (a)* **1982,** *71* (2), 505-510.

(29) Charoenphakdee, A.; Kurosaki, K.; Muta, H.; Uno, M.; Yamanaka S. Thermal Conductivity of the Ternary Compounds: AgMTe$_2$ and AgM_5Te$_8$ (M = Ga or In). *Mater. Trans.* **2009,** *50* (7), 1603-1606.

(30) Spitzer, D. P. Lattice Thermal Conductivity of Semiconductors: A Chemical Bond Approach. *J. Phys. Chem. Solids* **1970,** *31* (1), 19-40.

(31) Birch, F. The Velocity of Compressional Waves in Rocks to 10 kilobars: 2. *J. Geophys. Res.* **1961,** *66* (7), 2199-2224.

(32) Slack, G. A.; Tsoukala, V. G. Some Properties of Semiconducting IrSb$_3$. *J. Appl. Phys.* **1994,** *76* (3), 1665-1671.

(33) Cahill, D. G.; Pohl, R. O. Lattice Vibrations and Heat Transport in Crystals and Glasses. *Ann. Rev. Phys. Chem.* **1988**, *39* (1), 93-121.

(34) May, A. F.; Snyder G. J. Chapter 11-Introduction to Modeling Thermoelectric Transport at High Temperatures. In *Materials, Preparation, and Characterization in Thermoelectrics*; Rowe D. M., Ed.; CRC Press: Boca Raton, Florida, USA: **2012**; 11-4.

(35) Samanta, M.; Roychowdhury, S.; Ghatak, J.; Perumal, S.; Biswas, K. Ultrahigh Average Thermoelectric Figure of Merit, Low Lattice Thermal Conductivity and Enhanced Microhardness in Nanostructured $(GeTe)_x(AgSbSe_2)_{100-x}$. *Chem. Eur. J.* **2017**, *23* (31), 7438-7443.

(36) Shen, J.; Chen, Z.; lin, S.; Zheng, L.; Li, W.; Pei, Y. Single Parabolic Band Behavior of Thermoelectric p-Type CuGaTe$_2$. *J. Mater. Chem. C* **2016,** *4* (1), 209-214.

(37) May, A. F.; Toberer, E. S.; Saramat, A.; Snyder, G. J. Characterization and Analysis of Thermoelectric Transport in n-Type $Ba_8Ga_{16-x}Ge_{30+x}$. *Phys. Rev. B* **2009,** *80* (12), 125205.

(38) Bardeen, J.; Shockley, W. Deformation Potentials and Mobilities in Non-Polar Crystals. *Phys. Rev.* **1950,** *80* (1), 72-80.

(39) Pei, Y.; Shi, X.; LaLonde, A.; Wang, H.; Chen, L.; Snyder, G. J. Convergence of Electronic Bands for High Performance Bulk Thermoelectrics. *Nature* **2011,** *473*, 66-69.

(40) Tang, Y.; Gibbs, Z. M.; Agapito, L. A.; Li, G.; Kim, H.-S.; Nardelli, Marco B.; Curtarolo, S.; Snyder, G. J. Convergence of Multi-valley Bands as the Electronic Origin of High Thermoelectric Performance in $CoSb_3$ Skutterudites. *Nat. Mater.* **2015,** *14*, 1223-1228.

(41) Liu, W.; Tan, X.; Yin, K.; Liu, H.; Tang, X.; Shi, J.; Zhang, Q.; Uher, C. Convergence of Conduction Bands as a Means of Enhancing Thermoelectric Performance of *n*-Type $Mg_2Si_{1-x}Sn_x$ Solid Solutions. *Phys. Rev. Lett.* **2012,** *108* (16), 166601.

(42) Pei, Y.; Wang, H.; Snyder, G. J. Band Engineering of Thermoelectric Materials. *Adv. Mater.* **2012,** *24* (46), 6125-6135.

(43) Cutler, M.; Mott, N. F. Observation of Anderson Localization in an Electron Gas. *Phys. Rev.* **1969,** *181* (3), 1336-1340.

(44) Jain, A.; Ong, S. P.; Hautier, G.; Chen, W.; Richards, W. D.; Dacek, S.; Cholia, S.; Gunter, D.; Skinner, D.; Ceder, G.; Persson, K. A. Commentary: The Materials Project: A Materials Genome Approach to Accelerating Materials Innovation. *APL Materials* **2013,** *1* (1), 011002.

(45) Dresselhaus, M. S., Solid State Physics Part II: Optical Properties of Solids vol. 6. **2001**.

Chalcopyrite $ZnSnSb_2$: A Promising Thermoelectric Material

TOC figure